*Supplement of*

# Summertime ozone sensitivity to temperature in China: observational evidence and mechanistic attribution in urban and rural areas in the Yangtze River Delta region

Chang Su et al.

**Model tuning description**

All tuning experiments were conducted under a common set of baseline environmental conditions representative of JJA 2022 averages in the Yangtze River Delta (YRD): T = 30 °C, q = 0.0184 kg $kg^{-1}$, RH = 70 %, surface pressure = 100 kPa, PBL height = 590 m. Initial chemical fields were taken from the prescribed UKCA ST_urban configuration (Table S5), with localised adjustments for species most directly controlling $O_3$ chemistry ($NO_x$, CO, key VOCs, radicals; see Table S5). All other species were set to a negligible background value of $10^{-15}$ kg $kg^{-1}$. The UKCA chemistry framework used here follows published UKCA/UKESM descriptions {Archibald, 2020 #39}.

Each tuning experiment was integrated for 1 model year with a chemical time step of 10 minutes. Solar radiation was prescribed as a repeating diurnal cycle for 1 July 2022, with separate solar geometries for Shanghai (31.17 °N, 121.42 °E) and Lishui (28.30 °N, 119.56 °E). Model configurations used the Ori settings, in which temperature is held constant, and $C_5H_8$ emissions vary only with the diurnal solar cycle.

To prevent an unrealistically high buildup of long-lived species, any species not involved in rapid photochemistry that showed substantial concentration growth over two months was fixed at a constant value. These fixed values (Table S4) were taken from the ST_urban configuration (Table S5).

1. Initial tuning: NO and $C_5H_8$ emissions

   We prescribe NO anthropogenic emissions from the CEDS inventory and $C_5H_8$ biogenic emissions from MEGAN (Wu et al., 2020). The CEDS flux uses the 2022 JJA monthly-mean fluxes averaged over the target regions (grey cells in Fig. 2a–b in the main content), and the MEGAN flux is described by Fig. S1. These prescribed NO and $C_5H_8$ fluxes represent the primary $O_3$ precursor inputs during the initial tuning stage (units kg $m^{-2}$ $s^{-1}$, following the standard UKCA emission specification).

   **Step 1a (QSS / "variation removal").** Because the box configuration omits transport and initially excluded deposition, constrained precursors exhibited drift. We therefore first sought a **quasi-steady state (QSS)** for NO concentration ([NO]) and $C_5H_8$ concentration ([$C_5H_8$]) by iteratively scaling NO emissions and/or isoprene emissions (coarse factors first, then smaller adjustments). QSS was defined as: for ≥30 consecutive days, the day-to-day changes of the daily-mean [NO] and [C5H8] are <0.1%.

   **Step 1b (constraint matching).** After QSS was achieved, emissions were adjusted to match observational constraints: $[NO2]_{sim} \approx [NO2]_{obs}$, $[C5H8]_{sim} \approx [C5H8]_{obs}$ using $NO_2$ and $C_5H_8$ as proxies for the NOx and isoprene pools (NO was not observed at the study sites). Acceptance required $| C_{sim} - C_{obs} | / C_{obs} \leq 0.30$ for each constrained species (statistics matched to the observational averaging used in Table S1).

2. Adding and tuning additional emissions

   After primary tuning, additional emissions were introduced and tuned to re-establish QSS and match constraints under a more realistic precursor mix. Added emissions comprised anthropogenic CO emissions and selected anthropogenic VOC emissions ($C_2H_6$, $C_3H_8$, HCHO; selected based on CEDS availability and the UKCA ST chemical scheme) and biogenic monoterpene emissions from MEGAN.

   **Step 2a (QSS after adding emissions).** QSS was re-established for the extended system by sequentially scaling VOC emissions to stabilise the emitted VOC pool in order of $C_2H_6$, $C_3H_8$, Monoterp, HCHO, and $C_5H_8$, followed by scaling CO emissions to stabilise [CO] and scaling NO emissions to stabilise [NO]. The QSS criterion remained: <0.1% day-to-day change of daily-mean concentrations for ≥30 days.

   **Step 2b (constraint matching).** Emissions were then iteratively tuned to match [$NO_2$] [$C_5H_8$] [CO] and [HCHO] observations within ±30% (relative difference), with VOC emissions adjusted jointly to satisfy the HCHO constraint.

3. Adding and tuning deposition

To represent unresolved outfluxes (surface deposition and, implicitly, non-represented transport losses), **dry deposition** was enabled for $O_3$, CO, HCHO, and the $NO_y$ species ($NO_2$, $NO_3$, $N_2O_5$, $HO_2NO_2$, $HNO_3$, PAN, PPAN and MPAN) using the Wesely resistance framework as implemented in UKCA.

Deposition velocities were initialised from the UKCA/Wesely parameterisation as **24 h summer-mean** values assuming a surface mixture of 50% forest and 50% grass. Deposition was then tuned jointly with emissions to satisfy the same observational constraints while keeping emissions close to their inventory "priors" (CEDS for anthropogenic species; MEGAN for biogenic species).

In practice, [$NO_2$] was matched by jointly adjusting NO emissions and $NO_2$ deposition while using $NO_y$ deposition to represent additional $NO_x$ loss pathways and avoid unrealistically large adjustments to $NO_2$ deposition alone. Analogous joint tuning was applied for isoprene, HCHO, and CO (emissions + deposition) until all constrained species were within ±30% of observations.

Note: at this step, we tolerate $NO_2$ concentrations lower than those observed at the stations in Lishui while strictly constraining [$C_5H_8$] to within ±30% observations, on the grounds that the available measurements are from several monitoring sites in populated areas that behave as local urban environments, whereas the box model is intended to represent a wider, forest-surrounded rural background.

4. Determination of spin-up length for sensitivity experiments

A convergence-based spin-up length was determined for subsequent sensitivity experiments. For each candidate day N, daily-mean concentrations on day N were compared with those on day N+30 for [$O_3$], [$O(^3P)$], [OH], [$HO_2$], [$NO_2$], [$C_5H_8$], [CO], [HCHO]. he **earliest** day NNN for which all tracked species satisfied $|C(N+30)-C(N)|/C(N)<0.03$ was defined as the **convergence day**. The period from day 1 to day N was then used as the target spin-up (run length) for sensitivity experiments.

**Limitations of the box-model tuning and justification of the final configuration**

Ideally, a completed tuning procedure would retain anthropogenic and biogenic emissions close to their prior prescribed fluxes from CEDS and MEGAN, while dry-deposition velocities would exceed those recorded in the Wesely resistance scheme to account for both deposition and physical transport loss.

In practice, the absence of transport, clouds and wet removal in the UKCA Box configuration imposes constraints and compromises, which differ between the Shanghai and Lishui setups.

Shanghai (urban): tuning compromises and justification

1. BVOC emissions

Isoprene and monoterpene emissions were tuned to values larger than the original MEGAN fluxes. This behaviour reflects a combination of the coarse native spatial resolution (due to the low image resolution of the online journal figure; See Fig. S1) of the MEGAN fields over Shanghai and the compensation for missing anthropogenic VOC classes (e.g., aromatics) in the ST chemical scheme. These BVOC emissions could not be reduced simply by adjusting deposition, because only a small subset of VOCs (primarily HCHO) is deposited in the scheme.

2. Alkane emissions and VOC deposition

Emissions of $C_2H_6$ and $C_3H_8$ were tuned below their CEDS values, and no explicit dry deposition was applied to these alkanes (only to HCHO among the VOCs). In principle, one might adjust individual VOC fluxes while preserving the total VOC source, but in practice, increasing alkane emissions and reducing BVOC emissions led to unrealistically low $C_5H_8$ concentrations, violating the tuning criterion of matching observed mean BVOC levels.

3. $NO_x$ emissions and deposition

NO emissions were tuned to values below the CEDS inventory to avoid excessive $NO_x$ and $O_3$ build-up in the clear-sky, no-transport box configuration. In principle, part of this discrepancy could be

absorbed by increasing $NO_x$ deposition, but the implemented sink acts primarily on NO rather than $NO_2$, and enhancing $NO_2$ deposition tends to drive $NO_2$ unrealistically low. We therefore retain reduced NO emissions and only modest $NO_x$ deposition as a pragmatic representation of combined surface and export losses in the urban box.

4. CO emissions and deposition

   CO emissions can be tuned back towards the CEDS values, but doing so requires very large CO deposition velocities, which are difficult to justify physically. We therefore accept a residual CO emission adjustment as a limitation of the ST scheme in the box configuration and avoid imposing unrealistically strong CO deposition.

Overall, for Shanghai, we interpret the tuned configuration as follows. For VOCs, we use HCHO as an indicator of the effective VOC reactivity and consider the combined VOC burden to be within an acceptable range (see Table S1a), attributing the elevated BVOC fluxes primarily to the coarse MEGAN representation and missing anthropogenic VOC classes. For $NO_x$, the reduced NO emissions are viewed as partially compensating for the enhanced photochemistry in the clear-sky, no-transport box, which allows lower $NO_x$ to sustain the observed $O_3$ levels.

Lishui (Rural) tuning

1. VOC emissions

   All VOC emissions remain at their CEDS/MEGAN values except for $C_5H_8$, which is tuned below the MEGAN flux. This reduction cannot be offset via deposition because $C_5H_8$ is not deposited in the scheme. We attribute this adjustment mainly to the coarse-resolution MEGAN fields in a heterogeneous, forest-dominated rural region.

2. $NO_x$ emissions and deposition

   NO emissions are again reduced relative to CEDS. Increasing $NO_2$ deposition to compensate would readily drive $NO_2$ below the observed levels, so we limit the use of $NO_x$ deposition and accept a moderate downward adjustment of NO emissions.

Overall, for the LS tuning results, we justify it as:

For Lishui, the tuning adjustments are comparatively small. We tolerate $O_3$ and $NO_2$ concentrations lower than those observed at the station in the final deposition-tuned configuration, on the grounds that the available measurements are from several monitoring sites in populated areas that behave as local urban environments, whereas the box model is intended to represent a wider, forest-surrounded rural background. In such a setting with strong BVOC emissions and relatively sparse anthropogenic $NO_x$ sources, we expect the true area-mean $O_3$ and $NO_2$ levels to be lower than those at the urbanised monitoring sites. During the deposition-tuning phase, we therefore prioritised limiting the temporal variability of $O_3$ and $NO_2$ rather than forcing an exact match to the observed means.

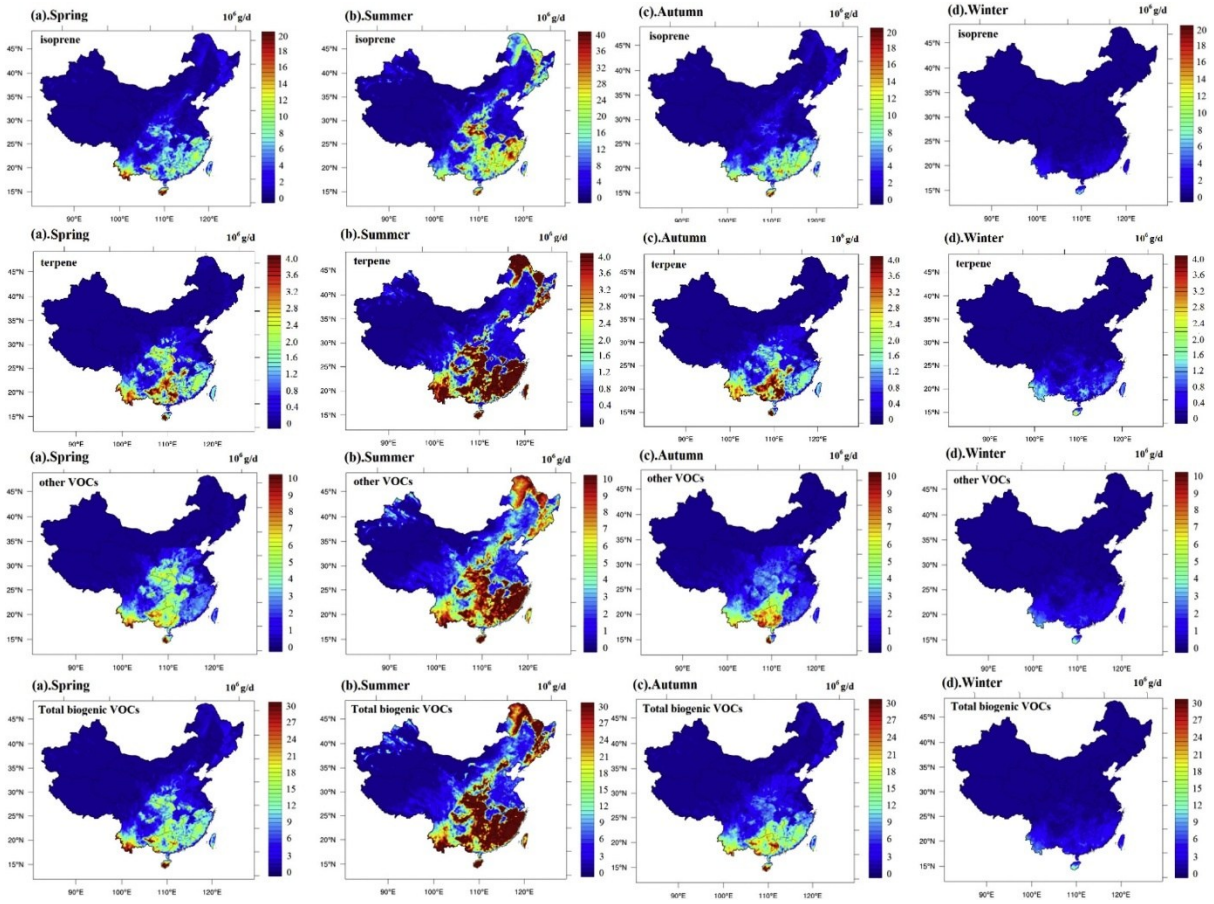


**Figure S1.** Monthly BVOC (four types) emissions in China in 2017 simulated by MEGAN with a 27-km horizontal grid spacing domain (Wu et al., 2020)

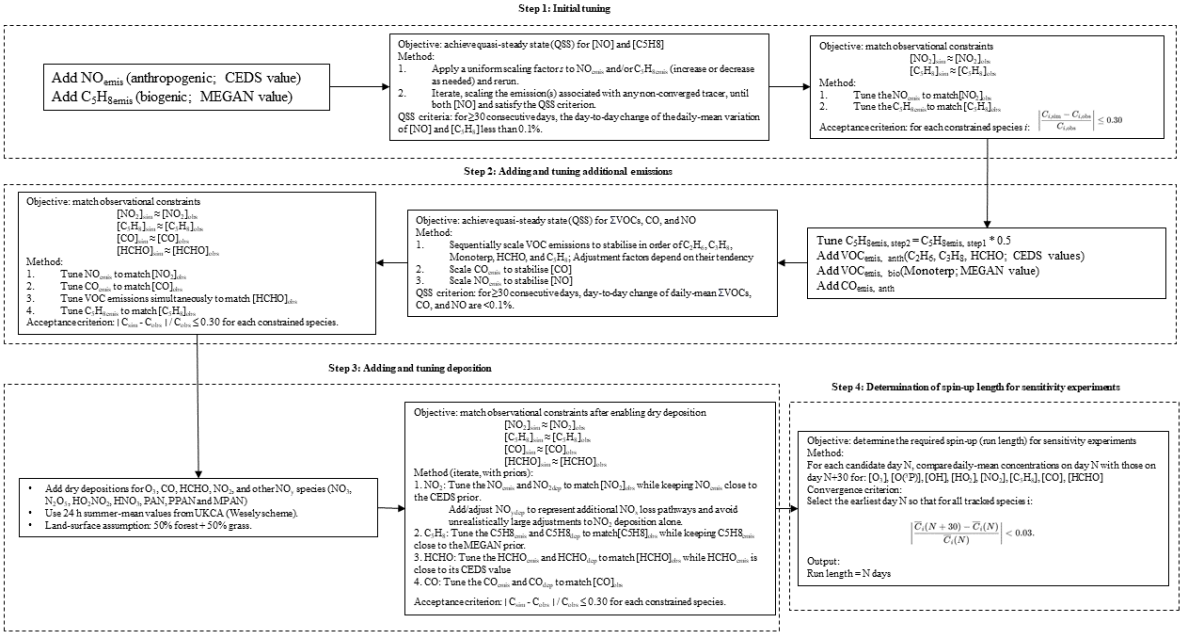


**Figure S2.** Flowchart for model tuning

**Table S1(a).** Model initialisation values (model input) and output results in Shanghai 2022 summer, and comparison with CMAS*, UKESM, and observation data from other studies

**Unit:(kg/kg)**

| Species | Model input | CMAS* | UKESM | Model output | Observation from other studies | Source, period, and location |
|---|---|---|---|---|---|---|
| $O_3$ | 7.44E-08 | 7.20E-08 | 1.16E-07 | 7.12E-08 | 7.40E-8(87.5 ug/m3) | CNEMC**, summer 2022, Shanghai |
| $NO_2$ | 1.68E-08 | 3.01E-08 | 2.50E-08 | 2.02E-08 | 1.74E-8(20.6 ug/m3) | CNEMC, summer 2022, Shanghai |
| CO | 5.37E-07 | 3.89E-07 | N/A | 5.42E-07 | 4.88E-7(581 ug/m3) | CNEMC, summer 2022, Shanghai |
| HCHO | 3.43E-09 | 3.92E-09 | N/A | 3.03E-09 | 3.43E-9(3.31 ppbv) | Guo et al., 2021, Jun-Aug 2018, Shanghai |
| $C_5H_8$ | 7.00E-10 | 1.47E-09 | 2.04E-09 | 2.86E-10 | 7.1E-10(0.3ppbv) | Gu et al. (2022), Jul 2018, Shanghai |
| PAN | 1.75E-09 | 2.59E-09 | 3.36E-09 | 7.34E-09 | 3.76E-9(0.9 ppbv) | Zhang et al. (2021), summer 2017, Shanghai |
| OH | 9.69E-14 | 9.46E-14 | 8.04E-13 | 1.08E-13 | 2.5E-13(1.02 * 10^7 cm-3) | Nan et al. (2017), Apr-Aug 2013, Shanghai |
| $HO_2$ | 1.24E-11 | N/A | 8.35E-11 | 1.25E-11 | 3.6E-12(0.8 * 10^8 cm-3) | Zhang et al. (2022), Nov-Dec 2019, Shanghai |

**Table S1(b).** Model initialisation values (model input) and output results in Lishui 2022 summer, and comparison with CMAS*, UKESM, and observation data from other studies

Unit:(kg/kg)

| Species | Model input | CMAS* | UKESM | Model output | Observation from other studies | Source, period, and location |
|---|---|---|---|---|---|---|
| $O_3$ | 4.67E-08 | 5.80E-08 | 1.06E-07 | 3.40E-08 | 4.67E-8(55.2 ug/m3) | CNEMC, summer 2022, Lishui |
| $NO_2$ | 1.43E-08 | 1.46E-08 | 3.52E-09 | 1.14E-09 | 1.43E-8(16.9 ug/m3) | CNEMC, summer 2022, Lishui |
| CO | 3.68E-07 | 2.62E-07 | N/A | 4.22E-07 | 3.68E-7(438 ug/m3) | CNEMC, summer 2022, Lishui |
| HCHO | 3.43E-09 | 6.35E-09 | N/A | 5.69E-09 | N/A | N/A |
| $C_5H_8$ | 7.00E-10 | 2.19E-08 | 5.17E-09 | 7.41E-09 | 5.2E-9 (1 to 3 ppbv) | Geng et al. (2011), Sep 2009, Lishui |
| PAN | 1.75E-09 | 3.85E-09 | 2.98E-09 | 3.22E-09 | 1.57E-9 (0.375 ppbv) | Xu et al. (2024), summer 2020, Nanjing |
| OH | 9.69E-14 | 4.84E-14 | 4.43E-14 | 1.05E-14 | 2.4E-13 (1.0×10^7 cm-3) | Ma et al. (2022), May-Jun 2018, Taizhou |
| $HO_2$ | 1.24E-11 | N/A | 1.83E-11 | 2.77E-11 | 5.2E-11 (1.1×10^9 cm-3) | Ma et al. (2022), May-Jun 2018, Taizhou |

*CAMS refers to CAMS (Copernicus Atmosphere Monitoring Service) global reanalysis. Specifically, it is the monthly-averaged fields from the EAC4 (European Centre for Medium-Range Weather Forecasts (ECMWF) Atmospheric Composition Reanalysis 4) dataset.

**CNEMC refers to ground-level hourly O3 observation data from the China National Environmental Monitoring Center (CNEMC).

**Table S2(a).** Model emissions tuning in Shanghai, 2022 summer

| Emitted Species | CEDS Emissions (kg m-2 s-1) | Adjustment | Model Emissions (kg m-2 s-1) |
|---|---|---|---|
| CO | 1.86E-08 | 0.045 | 8.37E-10 |
| NO | 1.17E-09 | 0.5 | 5.85E-10 |
| C2H6 | 2.02E-11 | 0.5 | 1.01E-11 |
| C3H8 | 1.83E-11 | 0.4 | 7.32E-12 |
| HCHO | 7.62E-12 | 1 | 7.62E-12 |
| C5H8* | 6.35E-11 | 2 | 1.27E-10 |
| Monoterp* | 6.35E-12 | 4 | 2.54E-11 |

**Table S2(b).** Model emissions tuning in Lishui, 2022 summer

| Emitted Species | CEDS Emissions (kg m-2 s-1) | Adjustment | Model Emissions (kg m-2 s-1) |
|---|---|---|---|
| CO | 2.61E-10 | 0.05 | 1.31E-11 |
| NO | 3.83E-11 | 0.5 | 1.91E-11 |
| C2H6 | 1.61E-12 | 1 | 1.61E-12 |
| C3H8 | 8.10E-13 | 1 | 8.10E-13 |
| HCHO | 3.98E-13 | 1 | 3.98E-13 |
| C5H8* | 4.45E-10 | 0.5 | 2.22E-10 |
| Monoterp* | 6.35E-11 | 1 | 6.35E-11 |

*$C_5H_8$ and Monoterpenes emissions are from MEGAN (Wu et al., 2020)

**Table S3(a).** Model depositions tuning in Shanghai, 2022 summer

| Deposited Species | Original deposition velocity (cm s-1) | Adjustment | Model deposition velocity (cm s-1) |
|---|---|---|---|
| O3 | 6.20E-03 | 1 | 6.20E-03 |
| CO | 3.00E-04 | 4 | 1.20E-03 |
| HCHO | 7.20E-03 | 1 | 7.20E-03 |
| NO2 | 3.95E-03 | 5 | 1.98E-02 |
| NO3 | 3.95E-03 | 1 | 3.95E-03 |
| N2O5 | 2.75E-02 | 1 | 2.75E-02 |
| HO2NO2 | 1.80E-02 | 1 | 1.80E-02 |
| HONO2 | 1.80E-02 | 1 | 1.80E-02 |
| PAN | 3.15E-03 | 1 | 3.15E-03 |
| PPAN | 3.15E-03 | 1 | 3.15E-03 |
| MPAN | 3.15E-03 | 1 | 3.15E-03 |

**Table S3(b).** Model depositions tuning in Lishui, 2022 summer

| Deposited Species | Original deposition velocity (cm s-1) | Adjustment | Model deposition velocity (cm s-1) |
|---|---|---|---|
| O3 | 6.20E-03 | 1 | 6.20E-03 |
| CO | 3.00E-04 | 2 | 6.00E-04 |
| HCHO | 7.20E-03 | 1 | 7.20E-03 |
| NO2 | 3.95E-03 | 1 | 3.95E-03 |
| NO3 | 3.95E-03 | 1 | 3.95E-03 |
| N2O5 | 2.75E-02 | 1 | 2.75E-02 |
| HO2NO2 | 1.80E-02 | 1 | 1.80E-02 |
| HONO2 | 1.80E-02 | 1 | 1.80E-02 |
| PAN | 3.15E-03 | 1 | 3.15E-03 |
| PPAN | 3.15E-03 | 1 | 3.15E-03 |
| MPAN | 3.15E-03 | 1 | 3.15E-03 |

**Table S4.** Long-lived fix species

| Fixed Species | Fixed Concentration (kg kg-1) |
|---|---|
| CH4 | 9.72E-07 |
| MeBr | 7.04E-11 |
| H2 | 1.00E-08 |
| CS2 | 1.00E-15 |
| COS | 1.00E-15 |

**Table S5.** UKCA ST_urban tracer initial configuration and conditions in Shanghai and Lishui

| Species | Shanghai | Lishui |
|---|---|---|
| O(3P) | 3.00E-16 | 3.00E-16 |
| O3* | 7.44E-08 | 4.67E-08 |
| N | 0.00E+00 | 0.00E+00 |
| NO | 6.90E-09 | 6.90E-09 |
| NO3 | 1.87E-12 | 1.87E-12 |
| NO2* | 1.68E-08 | 1.43E-08 |
| N2O5 | 1.21E-11 | 1.21E-11 |
| HO2NO2 | 1.61E-11 | 1.61E-11 |
| HONO2 | 9.16E-09 | 9.16E-09 |
| H2O2 | 1.96E-09 | 1.96E-09 |
| CH4 | 9.72E-07 | 9.72E-07 |
| CO* | 5.37E-07 | 3.68E-07 |
| HCHO* | 3.43E-09 | 3.43E-09 |
| MeOO | 3.32E-12 | 3.32E-12 |
| MeOOH | 3.29E-10 | 3.29E-10 |
| H | 1.29E-26 | 1.29E-26 |
| H2O | 1.84E-02 | 1.84E-02 |
| OH | 9.69E-14 | 9.69E-14 |
| HO2 | 1.24E-11 | 1.24E-11 |
| Cl | 4.43E-19 | 4.43E-19 |
| Cl2O2 | 7.40E-22 | 7.40E-22 |

| | | |
|---|---|---|
| ClO | 9.56E-17 | 9.56E-17 |
| OClO | 1.45E-19 | 1.45E-19 |
| Br | 1.20E-15 | 1.20E-15 |
| BrO | 7.36E-11 | 7.36E-11 |
| BrCl | 2.91E-19 | 2.91E-19 |
| BrONO2 | 2.50E-14 | 2.50E-14 |
| N2O | 4.86E-07 | 4.86E-07 |
| HCl | 3.98E-09 | 3.98E-09 |
| HOCl | 4.74E-14 | 4.74E-14 |
| HBr | 1.95E-12 | 1.95E-12 |
| HOBr | 1.27E-13 | 1.27E-13 |
| ClONO2 | 1.34E-15 | 1.34E-15 |
| CFCl3 | 1.82E-09 | 1.82E-09 |
| CF2Cl2 | 4.19E-09 | 4.19E-09 |
| MeBr | 7.04E-11 | 7.04E-11 |
| HONO | 2.96E-11 | 2.96E-11 |
| C2H6 | 2.17E-08 | 2.17E-08 |
| EtOO | 2.93E-13 | 2.93E-13 |
| EtOOH | 2.40E-11 | 2.40E-11 |
| MeCHO | 2.75E-10 | 2.75E-10 |
| MeCO3 | 1.11E-12 | 1.11E-12 |
| PAN | 1.75E-09 | 1.75E-09 |
| C3H8 | 6.03E-09 | 6.03E-09 |
| n-PrOO | 5.02E-14 | 5.02E-14 |
| i-PrOO | 1.32E-13 | 1.32E-13 |
| n-PrOOH | 5.02E-12 | 5.02E-12 |
| i-PrOOH | 9.78E-12 | 9.78E-12 |
| EtCHO | 2.51E-11 | 2.51E-11 |
| EtCO3 | 2.12E-14 | 2.12E-14 |
| Me2CO | 8.82E-09 | 8.82E-09 |
| MeCOCH2OO | 8.60E-14 | 8.60E-14 |
| MeCOCH2OOH | 1.09E-11 | 1.09E-11 |
| PPAN | 2.64E-11 | 2.64E-11 |
| MeONO2 | 7.89E-11 | 7.89E-11 |
| C5H8* | 7.00E-10 | 7.00E-10 |
| ISO2 | 6.32E-12 | 6.32E-12 |
| ISOOH | 1.39E-10 | 1.39E-10 |
| ISON | 1.84E-09 | 1.84E-09 |
| MACR | 3.04E-09 | 3.04E-09 |
| MACRO2 | 1.70E-12 | 1.70E-12 |
| MACROOH | 8.24E-11 | 8.24E-11 |
| MPAN | 1.63E-09 | 1.63E-09 |
| HACET | 2.59E-09 | 2.59E-09 |
| MGLY | 2.61E-10 | 2.61E-10 |
| NALD | 2.28E-10 | 2.28E-10 |
| HCOOH | 2.41E-10 | 2.41E-10 |
| MeCO3H | 1.91E-10 | 1.91E-10 |
| MeCO2H | 1.37E-10 | 1.37E-10 |

| | | |
|---|---|---|
| H2 | 1.00E-08 | 1.00E-08 |
| MeOH | 1.94E-08 | 1.94E-08 |
| DMS | 4.80E-11 | 4.80E-11 |
| SO2 | 3.91E-09 | 3.91E-09 |
| Monoterp* | 5.20E-10 | 5.20E-10 |

*Species' initial concentrations changed according to observations

## Supplementary References

Geng, F., et al.: Effect of isoprene emissions from major forests on ozone formation in the city of Shanghai, China, Atmos. Chem. Phys., 11, 10449-10459, 10.5194/acp-11-10449-2011, 2011.

Gu, C., et al.: Investigation on the urban ambient isoprene and its oxidation processes, Atmospheric Environment, 270, 118870, https://doi.org/10.1016/j.atmosenv.2021.118870, 2022.

Guo, Y., et al.: Atmospheric formaldehyde, glyoxal and their relations to ozone pollution under low- and high-NOx regimes in summertime Shanghai, China, Atmospheric Research, 258, 105635, https://doi.org/10.1016/j.atmosres.2021.105635, 2021.

Ma, X., et al.: OH and HO2 radical chemistry at a suburban site during the EXPLORE-YRD campaign in 2018, Atmos. Chem. Phys., 22, 7005-7028, 10.5194/acp-22-7005-2022, 2022.

Nan, J., et al.: Study on the daytime OH radical and implication for its relationship with fine particles over megacity of Shanghai, China, Atmospheric Environment, 154, 167-178, https://doi.org/10.1016/j.atmosenv.2017.01.046, 2017.

Sanderson, M. G., Collins, W. J., Hemming, D. L., and Betts, R. A.: Stomatal conductance changes due to increasing carbon dioxide levels: Projected impact on surface ozone levels, Tellus B: Chemical and Physical Meteorology, 59, 404-411, 10.1111/j.1600-0889.2007.00277.x, 2007.

Wesely, M. L.: Parameterization of surface resistances to gaseous dry deposition in regional-scale numerical models, Atmospheric Environment (1967), 23, 1293-1304, https://doi.org/10.1016/0004-6981(89)90153-4, 1989.

Wu, K., et al.: Estimation of biogenic VOC emissions and their corresponding impact on ozone and secondary organic aerosol formation in China, Atmospheric Research, 231, 104656, https://doi.org/10.1016/j.atmosres.2019.104656, 2020.

Xu, T., et al.: Investigation on the budget of peroxyacetyl nitrate (PAN) in the Yangtze River Delta: Unravelling local photochemistry and regional impact, Science of The Total Environment, 917, 170373, https://doi.org/10.1016/j.scitotenv.2024.170373, 2024.

Zhang, G., et al.: Simultaneous observation of atmospheric peroxyacetyl nitrate and ozone in the megacity of Shanghai, China: Regional transport and thermal decomposition, Environmental Pollution, 274, 116570, https://doi.org/10.1016/j.envpol.2021.116570, 2021.

Zhang, G., et al.: Observation and simulation of HOx radicals in an urban area in Shanghai, China, Science of The Total Environment, 810, 152275, https://doi.org/10.1016/j.scitotenv.2021.152275, 2022.